Available online at www.sciencedirect.com
SCIENCE DIRECT®
Journal of Solid State Chemistry 178 (2005) 3679–3685
JOURNAL OF SOLID STATE CHEMISTRY
www.elsevier.com/locate/jssc

Electronic behavior of three oxygen non-stoichiometric Fe^{4+}/Fe^{3+} oxoperovskites

H.D. Zhou*, J.B. Goodenough

Texas Materials Institute, ETC 9.102, 1 University Station, C2201, University of Texas at Austin, Austin, Texas 78712-1063, USA

Received 23 April 2005; received in revised form 6 September 2005; accepted 14 September 2005
Available online 11 October 2005

Abstract

For comparison with the Mn^{4+}/Mn^{3+} oxoperovskites at the crossover from localized to itinerant behavior of the σ-bonding e electrons, the electronic properties of three oxygen non-stoichiometric, mixed-valent Fe^{4+}/Fe^{3+} oxoperovskites were explored by measuring their resistivity $\rho(T)$, thermoelectric power $\alpha(T)$, and magnetic susceptibility $\chi(T)$. Oxidation of $Ca_2Fe_2O_5$ by annealing in ozone progresses by oxygen insertion to give conductive $CaFeO_3$ perovskite clusters in a localized-electron, weakly oxidized brownmillerite $Ca_2Fe_2O_{5+\delta}$ matrix. Removal of 0.12 oxygen per formula unit from $La_{1/3}Sr_{2/3}FeO_3$ lowers somewhat its cooperative disproportionation reaction, and fivefold-coordinated ions neighboring oxygen vacancies in the more ionically bonded slabs act as donors to the covalently bonded $Fe(V)O_6$ planes. Single-crystal $SrFeO_{2.83}$ exhibited bad-metal behavior with superparamagnetic, electron-rich fluctuations below 240 K that, on cooling below 190 K, become progressively trapped by the oxide-ion vacancies as an immobile second phase; long-range antiferromagnetic order is stabilized below a $T_N \approx 60$ K.

Keywords: Perovskites; Brownmillerite; Bad metals; Disproportionation; Oxygen insertion

1. Introduction

The octahedral-site Mn^{3+} ions of the $RMnO_3$ (R = rare earth) perovskites and the Fe^{4+} ions of the $AFeO_3$ (A = alkaline earth) perovksites each have a high-spin $3d^4$ manifold. The π-bonding t^3 manifold at each cation is localized with an atomic spin $S = \frac{3}{2}$. The σ-bonding e electron of the Mn^{3+}:t^3e^1 ion is also localized as is manifest by a cooperative ordering of the twofold-degenerate e orbitals, but the e electron of an Fe^{4+}:$t^3\sigma^{*1}$ ion occupies a narrow, itinerant-electron σ* band of e-orbital parentage. An intraatomic exchange field removes the spin degeneracy not only of the localized e orbitals at a Mn^{3+} ion, but also of the orbitally twofold-degenerate σ^*-band states at an Fe^{4+} ion. In the Mn^{4+}/Mn^{3+} and Fe^{4+}/Fe^{3+} mixed-valent perovskites, a crossover from localized to itinerant electron behavior may occur. Therefore, a meaningful comparison of the physical properties imparted by localized versus itinerant σ-bonding electrons in the Mn^{4+}/Mn^{3+} and Fe^{4+}/Fe^{3+} systems is possible and instructive. We distinguish the single-valent from the mixed-valent situations.

In $LaMnO_3$, which is representative of the single-valent $RMnO_3$ family, a cooperative site distortion below $T_{OO} = 750$ K removes the degeneracy of the localized e orbitals [1] whereas the orbital degeneracy of the σ* band of $CaFeO_3$ is removed below 290 K by the formation of molecular e orbitals within $Fe^{(4+\delta)+}O_6$ complexes that alternate with more ionically bonded $Fe^{(4-\delta)+}$ ions; δ approaches unity in an $Fe(V)O_6$ complex at $T = 0$ K [2]. The cost in on-site electron–electron electrostatic energy to form a localized Fe^{3+}:t^3e^2 configuration is, in this case, less than the gain in bonding energy within the $Fe(V)O_6$ complex. On the other hand, the orbital degeneracy of the σ* band is retained to lowest temperatures in $SrFeO_3$ where a RKKY indirect interatomic exchange interaction via itinerant σ* electrons gives a ferromagnetic spiral-spin configuration propagating along a [111] axis below $T_N = 134$ K [3].

*Corresponding author. Fax: +1 512 471 7681.
E-mail address: hdzhou@physics.utexas.edu (H.D. Zhou).

0022-4596/$ - see front matter © 2005 Elsevier Inc. All rights reserved.
doi:10.1016/j.jssc.2005.09.020

In the mixed-valent $R_{1-x}A_xMnO_3$ (A = alkaline earth) systems, the introduction of holes into the MnO_3 array creates a range of unusual phenomena that vary sensitively with x, temperature, and the mean size of the $R_{1-x}A_x$ ions as well as their ionic-size variance [4]. For example, holes introduced into the Mn^{4+}/Mn^{3+} couple of the $La_{1-x}Sr_xMnO_3$ system transform with increasing x from small polarons to two manganese (Zener) polarons that, on lowering the temperature, progressively condense into orbitally disordered, ferromagnetic clusters within an orbitally ordered matrix; these hole-rich, conductive clusters grow to beyond percolation below a global ferromagnetic Curie temperature T_C. Above T_C, the ferromagnetic clusters grow in an applied magnetic field at the expense of the orbitally ordered, paramagnetic matrix to give a colossal negative magnetoresistance at their percolation threshold. Below T_C, a vibronic conduction of the ferromagnetic phase transforms at $x>0.15$ into metallic conduction with e electrons occupying a narrow σ^* band of e-orbital parentage.

Oxygen-stoichiometric Fe(IV) oxides are synthesized under high oxygen pressure, and oxidation of the Fe^{5+}/Fe^{4+} redox couple is not accessible with conventional techniques. However, the introduction of holes or electrons into the Fe^{4+}/Fe^{3+} couple is accessible and provides an interesting comparison to the introduction of holes or electrons into the Mn^{4+}/Mn^{3+} couple. For example, $LaFeO_3$ is an antiferromagnetic insulator with $T_N = 750$ K [5], and holes introduced into the Fe^{4+}/Fe^{3+} couple of the $La_{1-x}Sr_xFeO_3$ system become trapped as hole pairs within molecular orbitals of $Fe(V)O_{6/2}$ complexes [6]. In $La_{1/3}Sr_{2/3}FeO_3$, Battle et al. [7] have reported and Matsuno et al. [8] have confirmed that below a first-order transition at 198 K, $Fe(V)O_{6/2}$ complexes order into every third (111) plane to give a charge-density wave (CDW)/SDW propagating along the [111] direction with a $q_{SDW} = 2q_{CDW}$; the formal valence and spins of the (111) planes change along the [111] direction as…353353…and…↑↑↑↓↓↓… On the other hand, the $La_{1/3}A_{2/3}MnO_3$ perovskites do not exhibit a disproportionation reaction. However, for $A = Ca$, a room-temperature CDW propagating along the orthorhombic [100] direction has been observed in films [9] to consist of charge-ordered slabs containing (formally) 50:50 Mn^{4+}/Mn^{3+} alternating with slabs of Mn^{4+} ions.

In this paper, we report the behavior of holes or electrons introduced into the Fe^{4+}/Fe^{3+} couple by oxygen non-stoichiometry. Several studies have already been made of $A^{2+}FeO_{3-\delta}$ iron oxides. Gibb et al. [10,11] used high oxygen pressure to introduce extra oxygen into the brownmillerite structure of $Ca_2Fe_2O_5$ and reported observing a disproportionation reaction in a $CaFeO_{2.60}$ sample, but not in a $CaFeO_{2.56}$ sample; Takano et al. [12] observed with Mössbauer spectroscopy the formation of $Fe^{3.5+}$–O–$Fe^{3.5+}$ pairs, i.e. Zener polarons with faster than 10^{-8} s e-electron transfer within an Fe^{3+}–O–Fe^{4+} pair, in vacancy-ordered $SrFeO_{2.86}$; and Nakamura et al. [13] have reported semiconductive conduction in $SrFeO_{3-\delta}$ samples having $\delta \geqslant 0.08$, but the critical value of δ at which the transition to metallic behavior in $SrFeO_3$ has not been determined. We have oxidized $Ca_2Fe_2O_5$ to $Ca_2Fe_2O_{5.16}$ by annealing the parent compound in ozone, and we have prepared single-crystal $SrFeO_{2.83}$ and $La_{1/3}Sr_{2/3}FeO_{2.88}$ by the traveling-solvent, floating-zone technique. The resistivity $\rho(T)$, the thermoelectric power $\alpha(T)$, and the magnetic susceptibility $\chi(T)$ have been used to track the behavior of the charge carriers.

2. Experimental

Polycrystalline $Ca_2Fe_2O_5$ was prepared by standard solid-state reaction. Stoichiometric mixtures of $CaCO_3$ (99.95%) and Fe_2O_3 (99.998%) were ground together and calcined in air at 950 °C for 24 h. The sample was then reground, cold-pressed into pellets, and sintered at 1200 °C for another 24 h in air and cooled to room temperature. Then the cold-pressed pellets of the as-prepared, red $Ca_2Fe_2O_5$ were put into a quartz tube and annealed at 500 °C with flowing ozone gas for 6 days. After this treatment, the color of the pellets changed to black, showing oxidation of the sample to $Ca_2Fe_2O_{5+\delta}$.

The feed and seed rods for the growth of single crystals of $SrFeO_{3-\delta}$ and $La_{1/3}Sr_{2/3}FeO_{3-\delta}$ were prepared by solid-state reaction. Stoichiometric mixtures of $SrCO_3/La_2O_3$ (99.95%) and Fe_2O_3 (99.998%) were ground together and calcined in air at 950 °C for 24 h. The sample was reground and sintered at 1150 °C for another 24 h in air and cooled to room temperature. It was then reground into a powder and pressed in a 6-mm-diameter × 60-mm rod under 400 atm hydrostatic pressure. The rods were finally sintered at 1300 and 1400 °C for 20 h in oxygen for $SrFeO_{3-\delta}$ and $La_{1/3}Sr_{2/3}FeO_{3-\delta}$, respectively. The crystal growth was carried out in an IR-heated image furnace (NEC) equipped with two halogen lamps and double ellipsoidal mirrors. The feed and seed rods were rotated in opposite directions at 25 rpm during crystal growth at a rate of 2 mm/h. An oxygen pressure of 2.0 bar was applied during growth.

Powder X-ray diffraction patterns for $Ca_2Fe_2O_5$, $Ca_2Fe_2O_{5+\delta}$, $SrFeO_{3-\delta}$, and $La_{1/3}Sr_{2/3}FeO_{3-\delta}$ were recorded with a Philips 1729 diffractometer equipped with a pyrolytic-graphite monochromater and CuK_α radiation; Si was the internal standard. Data were collected in steps of 0.020° over the range $20° \leqslant 2\theta \leqslant 80°$ with a count time of 15 s per step. Peak profiles were fitted with the program JADE. All samples were single-phase to XRD, Fig. 1. The lattice parameters are listed in Table 1.

A Perkin-Elmer TGA-7 thermogravimetric analyzer (TGA) was used to determine the oxygen content of the samples from the weight loss on reduction to Fe^0 on heating to 1000 °C in an H_2(5%)/Ar flow. The oxygen values were $Ca_2Fe_2O_{5.01(1)}$ for the as-prepared $Ca_2Fe_2O_5$, $Ca_2Fe_2O_{5.16(2)}$ for the ozone-annealed sample, and $SrFeO_{2.83(1)}$ and $La_{1/3}Sr_{2/3}FeO_{2.88(2)}$, for the two single crystals.

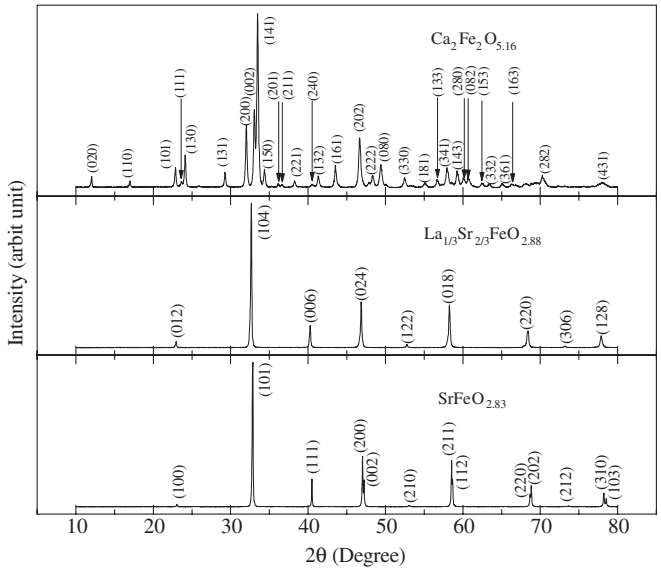

Fig. 1. Room-temperature XRD patterns for $Ca_2Fe_2O_{5.16}$, $La_{1/3}Sr_{2/3}FeO_{2.88}$, and $SrFeO_{2.83}$.

Table 1
Lattice parameters of samples

	Space group	a (Å)	b (Å)	c (Å)	Volume (Å^3)
$Ca_2Fe_2O_5$	*Pcmn*	5.604(1)	14.782(5)	5.432(2)	449.98
$Ca_2Fe_2O_{5.16}$	*Pcmn*	5.554(1)	14.912(5)	5.402(2)	447.40
$La_{1/3}Sr_{2/3}FeO_{2.88}$	*R-3c*	5.484(1)	5.484(1)	13.440(2)	350.06
$SrFeO_{2.83}$	*P4mm*	3.865(2)	3.865(2)	3.850 (3)	57.51

Magnetic-susceptibility was measured with a Quantum Design dc SQUID magnetometer after cooling in either zero field (ZFC) or in a measuring field (FC) of 2500 Oe.

The thermoelectric power $\alpha(T)$ was obtained with a laboratory-built apparatus as described elsewhere [14]. The resistivity was measured with a four-probe technique on single crystals or samples that were cold-pressed. The cold-pressing technique has been described elsewhere [15].

3. Results and discussion

3.1. $Ca_2Fe_2O_{5.16}$

3.1.1. Results

The as-prepared $Ca_2Fe_2O_5$ sample was orthorhombic *Pcmn* with $a = 5.604(1)$ Å, $b = 14.782(5)$ Å, $c = 5.432(2)$ Å, and $V = 449.98$ Å^3. After being annealed in ozone, $Ca_2Fe_2O_{5.16}$ keeps the orthorhombic *Pcmn* structure, but the lattice parameters changed to $a = 5.554(1)$ Å, $b = 14.912(5)$ Å, $c = 5.402(2)$ Å with a smaller volume $V = 447.40$ Å^3.

The as-prepared $Ca_2Fe_2O_5$ is a good insulator with so large a resistivity that we could not measure it with our apparatus. The resistivity of $Ca_2Fe_2O_{5.16}$ was smaller; the measured results are shown in Fig. 2(a). There is a peak around 250 K in the $d(\ln\rho)/d(1/T)$ vs. T curve, which signals a smooth change of the activation energy from 0.06 to 0.13 eV as the temperature increases. Fig. 2(b) shows the temperature dependences of the magnetic susceptibility $\chi(T)$ and its inverse, $1/\chi$, for $Ca_2Fe_2O_{5.16}$. There is an antiferromagnetic transition at $T_N = 110$ K, but the $1/\chi(T)$ curve above T_N does not obey a Curie–Weiss law. Fig. 2(c) shows that the thermoelectric power $\alpha(T)$ for $Ca_2Fe_2O_{5.16}$ is nearly temperature-independent above 250 K with a small negative value around -10 μV/K; it drops sharply below 250 K with decreasing temperature. For comparison, the magnetic susceptibility and the thermoelectric power of $Ca_2Fe_2O_5$ are also shown in the inset of Fig. 2(c). The thermoelectric power of $Ca_2Fe_2O_5$ shows typical semiconductor behavior with a large, positive value at 300 K of 320 μV/K. $Ca_2Fe_2O_5$ has an antiferromagnetic transition at 725 K [16]. We can fit the susceptibility data for $Ca_2Fe_2O_5$ below 150 K with the equation $\chi = \chi_0 + C/T$ with $\chi_0 = 0.0018$ emu/mol and $C = 0.005$ emuK/mol. If the increase of susceptibility below 150 K is presumably due to a paramagnetic species related to the existence of trapped Fe^{4+} ions, the concentration of Fe^{4+} ions can be estimated to be about 0.2% assuming $S = 2$ for Fe^{4+}; it would be less if the holes form superparamagnetic Zener polarons. This value is in the range of oxygen stoichiometry calculated from the TGA analysis.

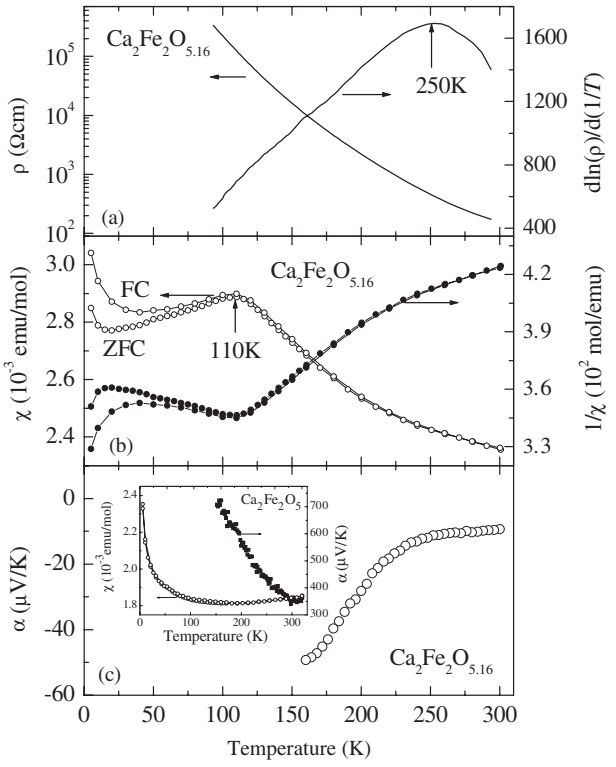

Fig. 2. Temperature dependences of (a) resistivtity $\rho(T)$ and $d(\ln\rho)/d(1/T)$; (b) molar magnetic susceptibility $\chi(T)$ and its inverse $1/\chi(T)$; and (c) thermoelectric power $\alpha(T)$ for $Ca_2Fe_2O_{5.16}$. Inset of (c): Temperature dependences of magnetic susceptibility $\chi(T)$ and thermoelectric power $\alpha(T)$ for $Ca_2Fe_2O_5$.

3.1.2. Discussion

Our ozone-annealed sample $Ca_2Fe_2O_{5.16}$ ($CaFeO_{2.58}$) contains about the same amount of excess oxygen as the $CaFeO_{2.56}$ and $CaFeO_{2.60}$ samples prepared by Gibb et al. [10,11] by annealing $Ca_2Fe_2O_5$ under 10 kbar O_2.

The observation of a negative thermoelectric power with 0.16 holes/Fe, Fig. 2(c), shows that the mobile holes are restricted to a subset of Fe atoms. Gibb et al. [10,11] have argued from Mössbauer data that the oxygen insertion into $Ca_2Fe_2O_5$ is in stages, oxygen diffusing preferentially into separated planes of tetrahedral sites to convert them into planes of octahedral-site iron. Although we were unable to identify such a staging in our samples with high-resolution electron microscopy, the Mössbauer data suggest segregation of oxygen-rich perovskite clusters three FeO_2 planes thick separated by a brownmillerite matrix. This model permits a qualitative explanation for an $\alpha(T)<0$. The holes have an octahedral-site preference energy. With two holes per three FeO_2 octahedra in an oxygen-rich perovskite clusters, the Fe(IV)/Fe(III) redox couple of a cluster would be one-third filled. Since the Fe(IV)/Fe(III) redox couple is pinned to the top of the O-2*p* bands, the partially filled *e* orbitals contain a large oxygen fraction, which allows direct communication between the perovskite clusters. Since the charge carriers belong to the one-third-filled Fe(IV)/Fe(III) redox couple of the clusters, direct communication between clusters would give an $\alpha(T)<0$. Moreover, stoichiometric $CaFeO_3$ undergoes a disproportionation reaction below 290 K, and a charge transfer below 250 K from electron-rich perovskite clusters to trap sites in the brownmillerite matrix is consistent with this observation.

The nearly temperature-independent thermoelectric power $\alpha(T)$ above 250 K in Fig. 2(c) as well as an activated $\rho(T)$ are consistent with a polaronic conduction of the perovskite electrons having a motional enthalpy in the mobility $\Delta H_m = 0.13$ eV. The sharp increase in the magnitude of $\alpha(T)$ below 250 K signals a trapping of electronic charge carriers from the perovskite clusters; given the octahedral-site preference of the Fe(IV), we attribute the electron traps to fivefold-coordinated Fe(IV) at isolated interstitial oxygen in the brownmillerite matrix. Transfer of electrons from the perovskite slabs to the brownmillerite Fe(IV) below 250 K would reduce the concentration of electronic charge carriers in the $CaFeO_3$ clusters, thereby increasing $|\alpha(T)|$. An associated reduction of the motional enthalpy of the charge carriers to $\Delta H_m = 0.06$ eV signals an approach to the itinerant character of the *e* electrons formed in stoichiometric $CaFeO_3$. Note that we do not attribute the activation energy of $\rho(T)$ above 250 K to an $E_a = \Delta H_m + (\Delta H_t/2) \approx 0.13$ eV, where $\Delta H_t = 0.14$ eV is an acceptor-state trapping energy below 250 K, because $\alpha(T)$ is temperature-independent above 250 K.

The magnetic data of Fig. 2 are also consistent with this two-phase model. The brownmillerite matrix would become antiferromagnetic well above room temperature, which makes meaningless interpretation of the magnetic susceptibility below room temperature with a paramagnetic Curie–Weiss law. On the other hand, the magnetic data of Fig. 2(b) clearly show an antiferromagnetic transition at a $T_N = 110$ K with a difference between the FC and ZFC measurements below T_N that is characteristic of a weak ferromagnetic component due to spin canting. We attribute this Néel temperature to the perovskite clusters; the perovskite $SrFeO_3$, which does not undergo a disproportionation reaction as does stoichiometric $CaFeO_3$, has a $T_N = 134$ K [3]. Long-range magnetic order between the perovskite clusters would be through the antiferromagnetic brownmillerite matrix. Since the perovskite clusters are also antiferromagnetic with only a weak ferromagnetic component, the situation is different from that of a classic spin glass. Nevertheless, the *M–H* hysteresis loop taken at 5 K, Fig. 3, shows only a small remanence and an effective magnetocrystalline anisotropy that is huge. These features signal a magnetic coupling between the magnetic order in the perovskite clusters and that of the brownmillerite matrix.

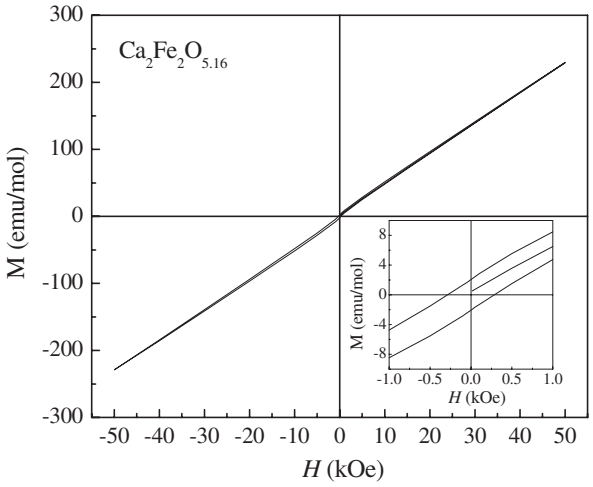

Fig. 3. *M–H* hysteresis loop at 5 K for $Ca_2Fe_2O_{5.16}$.

It is also noteworthy that the $1/\chi(T)$ curve shows a significant bending setting in below 250 K where the $\rho(T)$ and $\alpha(T)$ data signal a trapping out of electrons from the perovskite clusters.

3.2. $La_{1/3}Sr_{2/3}FeO_{2.88}$

3.2.1. Results

Fig. 4 shows the transport and magnetic data for $La_{1/3}Sr_{2/3}FeO_{2.88}$. Fig. 4(b) signals an antiferromagnetic transition at $T_N \approx 180$ K. Above 180 K, the thermoelectric power $\alpha(T)$ of Fig. 4(c) is essentially temperature-independent with a positive value of 13.5 μV/K; with decreasing temperature, it drops sharply below 180 K to a large negative value. The resistivity $\rho(T)$ of Fig. 4(a) is consistent with polaronic conduction above 180 K having a motional enthalpy $\Delta H_m = 0.07$ eV. The $d(\ln \rho)/d(1/T)$ curve of the

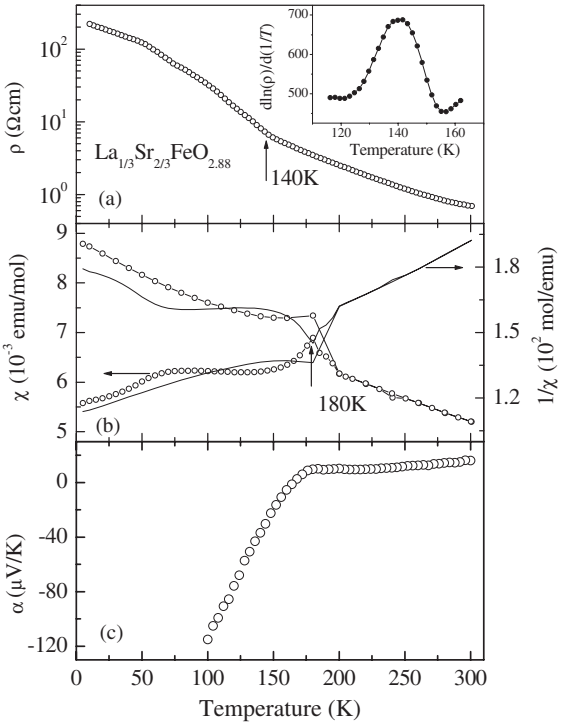

Fig. 4. Temperature dependences of (a) resistivtity $\rho(T)$; (b) molar magnetic susceptibility $\chi(T)$ and its inverse $1/\chi(T)$; and (c) thermoelectric power $\alpha(T)$ for $La_{1/3}Sr_{2/3}FeO_{2.88}$. Inset of (a): $d(\ln\rho)/d(1/T)$ vs. T curve for $La_{1/3}Sr_{2/3}FeO_{2.88}$.

inset of Fig. 4(a) reveals a change in the activation energy of $\rho(T)$ centered at 140 K.

3.2.2. Discussion

The introduction of 0.12 oxygen vacancies into $La_{1/3}Sr_{2/3}FeO_3$ changes the Fe(IV)/Fe ratio from 0.67 to 0.43. The $\alpha(T)$ and $\rho(T)$ data above 180 K signal the charge carriers are polaronic holes with a motional enthalpy $\Delta H_m = 0.07$ eV, which implies that the charge carriers are polaronic holes mobile over all the Fe atoms. To obtain experimentally the size of the polaronic holes, we assume the statistical term [17]

$$\alpha_s = (k/e)\ln[\beta(1-Qc)/Qc] \quad (1)$$

dominates the thermoelectric power. With a spin-degeneracy factor $\beta = 1$ due to the strong intraatomic exchange energy and $c = 0.43$ for the fraction of holes per Fe atom, the number of Fe sites occupied by a polaron is calculated to be $Q = 1$, which corresponds to the anticipated small dielectric polarons mobile over all Fe atoms at $T > 180$ K.

Since $La_{1/3}Sr_{2/3}FeO_3$ undergoes a cooperative disproportionation reaction $2Fe(IV)O_{6/2} = Fe(V)O_{6/2} + Fe^{3+}$ below a first-order transition at 198 K, we ask ourselves whether such a disproportionation reaction over a volume fraction of $La_{1/3}Sr_{2/3}FeO_{2.88}$ can account for the transition at 180 K in Fig. 4. The holes would be trapped out at the $Fe(V)O_{6/2}$ clusters, and the presence of oxygen vacancies would introduce electrons. Since the Fe^{3+}/Fe^{2+} redox couple is removed from the Fe^{4+}/Fe^{3+} redox couple by a large intraatomic energy $U_{eff} = U + \Delta_{ex}$, any electrons introduced would occupy the $Fe(V)O_{6/2}$ cluster orbitals as $Fe(IV)O_{6/2}$ units formed by cooperative oxygen displacements responsible for the

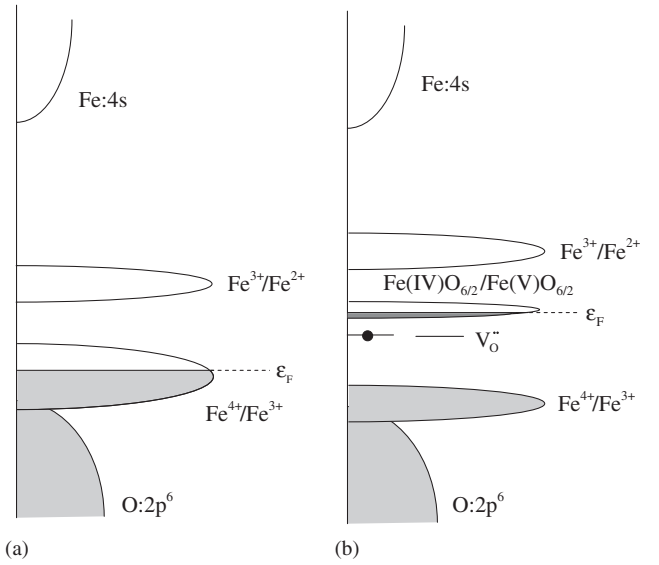

Fig. 5. Schematic energy diagrams for $La_{1/3}Sr_{2/3}FeO_{2.88}$ with (a) $T > 180$ K; (b) $T < 180$ K. $V_O^{\bullet\bullet}$ represents an oxygen vacancy containing two electrons if —●— or one electron if ——.

$$-Fe^{3+} - O - Fe(V) - O - Fe^{3+} - O - Fe^{3+} - \quad (2)$$

CDW. As illustrated schematically in Fig. 5(b), the (111) planes within a CDW would have short Fe–O bonds to give rise to a mixed-valent $Fe(V)O_{6/2}/Fe(IV)O_{6/2}$ level supporting n-type conduction. However, the n-type carriers would be progressively trapped out at oxygen vacancies in the more ionic regions as the temperature is lowered to give an increasing $|\alpha(T)|$. The transition at 180 K appears to be smooth with a progressive growth of the volume fraction of the CDW phase over the temperature interval $120\text{ K} < T < 180$ K.

3.3. $SrFeO_{2.83}$

3.3.1. Results

The resistivity $\rho(T)$ curve of single-crystal $SrFeO_{2.83}$ shows, inset of Fig. 6(a), a smooth metal-insulator transition near 190 K with a change in slope at ca. 240 K. Below 190 K, the Arrhenius plot of $\rho = \rho_o \exp(-E_a/kT)$ in Fig. 6(a) gives an activation energy $E_a = 0.02$ eV. Nakamura and Iida [13] reported a similar $E_a = 0.02$ eV for $SrFeO_{2.82}$, but they failed to observe a transition to metallic behavior in their polycrystalline sample.

Above 240 K, the inverse magnetic susceptibility, $1/\chi(T)$, of Fig. 6(b), is linear with a Weiss constant $\theta = 41$ K; below 240 K, the curve flattens in a manner typical of short-range magnetic ordering; long-range antiferromagnetic order sets in below a $T_N \approx 60$ K.

The thermoelectric power $\alpha(T)$ of Fig. 6(c) has a small, nearly temperature-independent negative value above

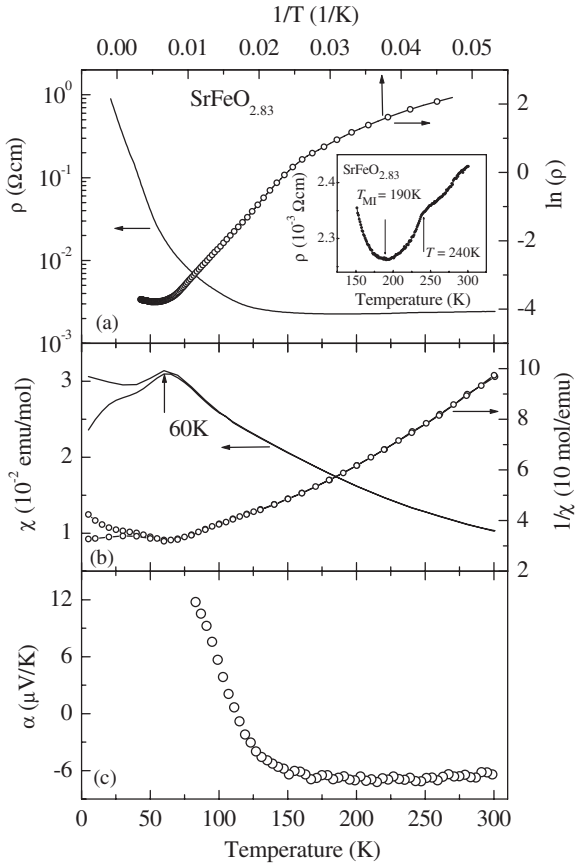

Fig. 6. (a) Temperature dependences of resistivtity ρ(T) and $\ln\rho$ vs $1/T$ curve; and temperature dependences of (b) molar magnetic susceptibility $\chi(T)$ and its inverse $1/\chi(T)$; and (c) thermoelectric power $\alpha(T)$ for $SrFeO_{2.83}$. Inset of (a): temperature dependences of resistivtity $\rho(T)$ with $150\,K < T < 300\,K$ for $SrFeO_{2.83}$.

240 K, $\alpha(T)$ rises sharply with decreasing temperature below 150 K.

3.4. Discussion

The σ-bonding e electrons of the high-spin Fe(IV) ions of $SrFeO_3$ occupy a narrow σ^* band of itinerant-electron states in which the spin degeneracy is removed by intraatomic exchange with the spin $S = \frac{3}{2}$ of a localized-electron, π-bonding t^3 manifold. Removal of 0.17 oxide ions introduces 0.34 electrons into the Fe^{4+}/Fe^{3+} redox couple, which would give an electronic conductivity if the electrons have access to all the Fe atoms. Since the oxygen vacancies strongly perturb the periodic potential of the $FeO_{3-\delta}$ array, the narrow σ^* band of $SrFeO_3$ would either develop Anderson-localized states at the wings of the σ^* band or be transformed into a polaronic conductor with a trapping out of electronic polarons at the oxygen vacancies as the temperature is lowered. So long as the Fermi energy remains above the mobility edge introduced by Anderson localization, the crystal should exhibit metallic behavior. Moreover, itinerant σ^* electrons would couple nearest-neighbor spins ferromagnetically by de Gennes double exchange to give a paramagnetic Weiss constant $\theta > 0$ [18]. Moreover, trapping of electrons at oxygen vacancies below 240 K would reduce the ferromagnetic coupling, thereby flattening the $1/\chi(T)$ curve by lowering the Weiss constant θ. However, the transition from n-type to p-type conduction would require, with this model, a transition from conduction in the matrix to conduction between interacting trap states at the oxygen vacancies, and trapping out of charge carriers should change $\alpha(T)$ in the range $190\,K < T < 240\,K$, which is not observed.

On the other hand, $SrFeO_{2.83}$ is a "bad metal," and the $\alpha(T)$ data above 240 K has little temperature dependence. These features are characteristic of the transport behavior of a mixed-valent perovskite at crossover from localized to itinerant electronic behavior with strong electron-lattice interactions, but no trapping into small polarons [4]. In this situation, an ordering at lower temperatures of the optical-mode lattice vibration that would trap electrons within molecular orbitals of a cluster of Fe atoms would manifest itself as a spinodal phase segregation into electron-rich and electron-poor phases. The simplest such electron-rich cluster would be a two-iron Fe^{3+}–O–Fe^{4+} pair corresponding to a Zener polaron; Zener polarons with zero motional enthalpy give rise to ferromagnetic Zener double exchange [19]. Thus bad-metal behavior would also give a paramagnetic Weiss constant $\theta > 0$. Moreover, an electron-rich cluster containing fast electron transfer would become superparamagnetic above a long-range ordering temperature.

To apply the Zener polaron model to account for the data of Fig. 6 for $SrFeO_{2.83}$, we point out that the appearance of short-range ferromagnetic fluctuations below 240 K would not only be responsible for the observed flattening of the paramagnetic $1/\chi(T)$ curve, but would also reduce spin-disorder scattering of the mobile electrons so as to account for the sharp change in the slope of $\rho(T)$ at 240 K. The $\alpha(T)$ data signal that the mobile electrons continue to have access to all the Fe atoms down to 190 K whereas the change from $\alpha(T) < 0$ to $\alpha(T) > 0$ on cooling below 110 K suggests a progressive condensation of the mobile Zener polarons into an electron-rich phase that is pinned by the oxygen vacancies to a minority volume fraction of the sample. However, in order for the other percolating volume fraction to be a p-type polaronic conductor, the electron-rich phase must capture a few electrons from the $SrFeO_3$ matrix.

4. Conclusions

Comparison of mixed-valent Mn^{4+}/Mn^{3+} and Fe^{4+}/Fe^{3+} oxoperovskites is instructive since transitions between itinerant and localized electronic behavior of the σ-bonding electrons in the presence of localized π-bonding electrons can be accessed in both. In the transitional compositions, strong electron–phonon interactions give rise to "bad metal" behavior at higher temperatures and spinodal phase segregation at lower temperatures into electron-rich and electron-poor regions, one region containing

molecular-orbital (or itinerant) electrons and the other localized electrons. On the approach to the transition from the itinerant-electron side, the Mn^{4+}/Mn^{3+} perovskites are ferromagnetic metals and cooperative orbital ordering is manifest as the σ^* band narrows. In contrast, the Fe^{4+}/Fe^{3+} perovskites have σ^* bands that either segregate into an electron-rich and an electron-poor phase or, as the band narrows, undergo the disproportionation reaction $2Fe(IV)O_{6/2} = Fe(V)O_{6/2} + Fe^{3+}$. Covalent bonding in the $2Fe(IV)O_{6/2}$ sited is too large for Jahn–Teller ordering of localized orbitals.

In this paper, we have explored the transitional domain in iron perovskites made oxygen non-stoichiometic. In those oxides, segregation into oxygen-rich and oxygen-poor phases can occur at relatively low temperatures and electrons are trapped from octahedral sites to sites of lower oxygen stoichiometry at oxygen vacancies below room temperature. Clustering of interstitial oxygen in ozone-oxidized $Ca_2Fe_2O_{5.16}$ was argued to provide a $CaFeO_3$ perovskite phase within a brownmillerite matrix that orders antiferromagnetic below 110 K, well below the Néel temperature of the brownmillerite matrix, which contains some isolated interstitial oxygen atoms. A single crystal of $La_{1/3}Sr_{2/3}FeO_{2.88}$ was argued to undergo a progressive growth, on cooling below 180 K, of a phase containing a CDW disproportionation reaction. A single crystal of $SrFeO_{2.83}$ was argued to segregate on cooling into two-iron Zener polarons that become superparamagnetic below 240 K; the Zener polarons become increasingly trapped into an electron-rich phase pinned at oxygen vacancies on cooling below 190 K.

Acknowledgments

The NSF and the Robert A. Welch Foundation of Houston, TX, are thanked for financial support.

References

[1] J.B. Goodenough, Phys. Rev. 100 (1955) 564;
J. Rodrigues-Carvajal, M. Hennion, F. Moussa, A.H. Moudden, L. Pinsard, A. Revcolevschi, Phys. Rev. B 57 (1998) R3189;
Y. Murakami, J.P. Hill, D. Gibbs, M. Blume, I. Koyama, M. Tanaka, H. Kawata, T. Arima, Y. Tokura, K. Hirota, Y. Endoh, Phys. Rev. Lett. 81 (1998) 582.
[2] M. Takano, N. Nakanishi, Y. Takeda, S. Naka, T. Takada, Mater. Res. Bull. 12 (1977) 923;
T. Takeda, R. Kanno, Y. Kawamoto, M. Takano, S. Kawasaki, T. Kamiyama, F. Izumi, Solid State Sci. 2 (2000) 673.
[3] P.K. Gallagher, J.B. McChesney, D.N.E. Buchanan, J. Chem. Phys. 41 (1964) 2429;
T. Takeda, S. Komura, H. Fugii, J. Magn. Magn. Mater. 31/34 (1983) 797.
[4] J.B. Goodenough, J.-S. Zhou, Struct. Bonding 98 (2001) 17.
[5] W.C. Koehler, E.O. Wollan, M.K. Wilkinson, Phys. Rev. 118 (1960) 58.
[6] S.E. Dann, D.B. Currie, M.T. Weller, M.F. Thomas, A.D. Alrawwas, J. Solid State Chem. 109 (1994) 134.
[7] P.D. Battle, T.C. Gibb, S. Nixon, J. Solid State Chem. 79 (1989) 75.
[8] J. Matsuno, T. Mizokawa, A. Fujimori, K. Mamiya, Y. Takeda, S. Kawasaki, M. Takano, Phys. Rev. B 60 (1999) 4605.
[9] S. Mori, C.H. Chen, S.-W. Cheong, Phys. Rev. Lett. 81 (1998) 3972.
[10] T.C. Gibb, A.J. Herod, D.C. Munro, N. Peng, J. Mater. Chem. 4 (1994) 1451.
[11] T.C. Gibb, A.J. Herod, D.C. Munro, N. Peng, J. Mater. Chem. 5 (1995) 1909.
[12] M. Takano, T. Okita, N. Nakayama, Y. Bando, Y. Takeda, O. Yamamoto, J.B. Goodenough, J. Solid State Chem. 73 (1988) 140.
[13] S. Nakamura, S. Iida, J. Appl. Phys. 34 (1995) L291.
[14] J.B. Goodenough, J.-S. Zhou, J. Chan, Phys. Rev. B 47 (1993) 5275.
[15] J.-S. Zhou, J.B. Goodenough, B. Dabrowski, Phys. Rev. B 67 (R) (2003) 020404.
[16] T. Takeda, Y. Yamaguchi, S. Tomiyoshi, M. Fukase, M. Sugimoto, H. Watanabe, J. Phys. Soc. Japan 24 (1968) 446.
[17] J.B. Goodenough, J. Solid State Chem. 1 (1970) 349.
[18] P.G. de Gennes, Phys. Rev. 118 (1960) 141.
[19] C. Zener, Phys. Rev. 82 (1951) 403.